Springer

KSME

Journal of Mechanical Science and Technology 24 (9) (2010) 1809~1818
www.springerlink.com/content/1738-494x
DOI 10.1007/s12206-010-0626-7

Numerical investigation of an axi-symmetric laminar jet impinging on a dimpled surface under uniform heat flux using a finite element method †

Koonlaya Kanokjaruvijit[1,*], Chakkraphan Thawonngamyingsakul[2] and Somchai Wongwises[3]

[1]*Department of Mechanical Engineering, Naresuan University, Phitsanulok 65000 Thailand*
[2]*Department of Mechanical Engineering, Rajamangala University of Technology Lanna Tak, Tak 63000, Thailand*
[3]*Department of Mechanical Engineering, King Mongkut's University of Technology Thonburi, Bangmod, Bangkok 10140 Thailand*

(Manuscript Received April 13, 2009; Revised March 17, 2010; Accepted May 11, 2010)

Abstract

The purpose of this study is to numerically investigate heat transfer and flow field in a semi-confined axi-symmetric laminar air jet impinging on a concave surface, or dimple, with uniform heat flux. A commercial software package relying on the finite element method was used for the simulation, and mesh convergence was examined in order to minimize computational cost. Jet impingement on a flat plate was used as a baseline reference case, and flat plate results were validated against previously published experimental data with good agreement. The effects of various parameters involved in dimple impingement –such as Reynolds number (Re) between 100–1,400; jet-to-plate spacing (H/D_j) ranging from 2 to 6 jet diameters; dimple depths (d/D_d) of 0.1, 0.15, and 0.2; and the ratio of jet diameter and dimple projected diameter (D_j/D_d) from 0.25 to 1– were all studied. Comparisons show that heat transfer reduction occurs in the presence of dimples because of the larger impingement area, which results in less momentum flux. The dimple curvature lifts the post-impinging fluid and creates a backflow, instead of allowing it to maintain contact with the surface, as is the case with flat plate impingement.

Keywords: Jet impingement ; Dimple ; Finite element

1. Introduction

Jet impingement is one of the most effective heat transfer augmenting techniques in heating, cooling, and drying applications. Although most articles related to jet impingement deal with turbulence, knowledge of its laminar flow is crucial in understanding the physics of turbulence, especially at the stagnation region where static pressure is sufficiently high to induce viscous effect in the turbulent jet. Bergthorson et al. [1] scrutinized a round impinging jet through experiments and numerical analysis using three formulas: axi-symmetric unsteady Navier-Stokes equations with the use of spectral-element method, potential-flow formulation using second-order centered finite difference, and streamfunction formulation. Results of their study, in the form of jet centerline velocities, were compared with the calculated results obtained from the current study. Angioletti et al. [2] examined heat transfer in laminar and transitional unconfined jet impingement between Reynolds numbers (Re) 1,000 and 4,000, experimentally and numerically. Different jet shapes have been investigated. Chattanopadhyay [3] employed the finite volume method and found 20% less heat transfer in an annular jet compared to a round jet. Furthermore, a three-dimensional three-by-three array of laminar impinging square jets with spent fluid removal was examined numerically by Aldabbagh and Sezai [4].

Dimples have been considered as heat transfer enhancers to jet impingement. However, heat transfer results were not consistent among the various studies. Azad et al. [5] found higher heat transfer results compared with those for flat plates for Re values between 4,850 and 18,300. Ekkad and Controvitz [6] reported that the presence of dimples resulted in a lower heat transfer for Re = 4,800–14,800. Kanokjaruvijit and Martinez-Botas [7-9] showed enhanced heat transfer in the presence of dimples with strong crossflows for Re = 5,000–11,500. None of these works gave detailed information on flow visualization.

This investigation started by validating the flow and heat transfer results of an axi-symmetric laminar jet impinging on a uniform heat flux surface, which was obtained from a calculation using the finite element method, against experimental results and those obtained from the finite difference method in literature. Using the flat plate impingement results as baseline cases, dimple impingement was studied together with various parametric effects, such as Re, jet-to-plate spacing (H/D_j), dimple depth (d/D_d), and ratio of nozzle exit diameter to dimple projected diameter (D_j/D_d). Due to the scarcity of informa-

† This paper was recommended for publication in revised form by Associate Editor Gihun Son

* Corresponding author. Tel.: +66 5526 1000, Fax: +66 5526 1062
E-mail address: koonlaya@gmail.com

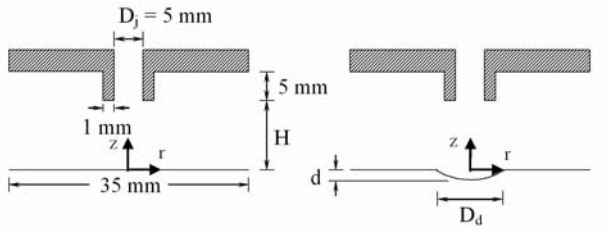

(a) Flat plate (b) Dimpled plate

Fig. 1. Dimension and tested parameters (not to scale).

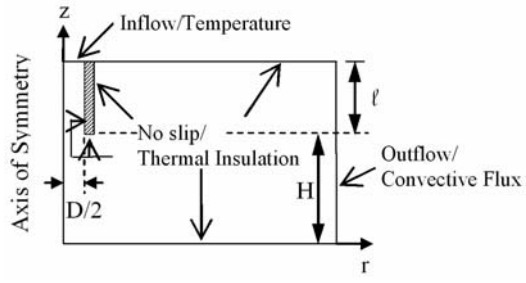

(a) Flat plate

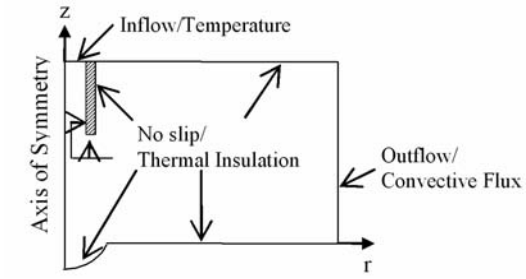

(b) Dimpled plate

Fig. 2. Dimensions and boundary conditions.

tion on heat transfer and flow of a laminar jet impinging onto a dimple, this study intends to provide computational data for better understanding of the experimental results found by previous researchers [5-9].

2. Numerical models

2.1 Computational domain

Fig. 1 shows sketches of the problem set-ups for the flat plate and dimple impingements with a jet diameter of 5 mm extruding from the nozzle plate and a nozzle wall of 1 mm thickness. Initially, the target plate is set at 35 mm long, but the domain is lengthened later in some cases in order to achieve valid results.

Because the problem is two-dimensional (2D) axisymmetric, the computational domain is reduced to half (Fig. 2), allowing for less time and memory usages. Throughout this investigation, a commercial software package for finite element analysis called COMSOL, which is available at the Naresuan University, is used. It pre-defines physical partial differential equations (PDEs) through multiphysics features. Hence, boundary conditions for both problems must be defined simultaneously as shown in the figure. For the flow problem, all solid walls are assigned "no-slip" conditions, which are mathematically written as $v_r = v_z = 0$. The nozzle exit, where the jet is issued, is given an "inflow" condition, $v = U_j$, assigned by the required jet velocity. The post impinging jet leaves the domain to go to the ambient environment. Thus, the domain end is assigned the "outflow" or "do nothing" boundary condition, which means the pressure of the boundary is zero.

Considering the heat transfer cases, an air jet with flat velocity profile at a temperature of 300 K is discharged through the nozzle, whose walls and adjacent walls are assigned by a Neumann boundary condition of "thermal insulation" or $\left.\frac{\partial T}{\partial r}\right|_{nozzle\ wall} = 0$. The target plate associated with heat transfer through the jet is given a constant heat flux of 500 W/m^2. The post-impinging jet leaves the domain to "convective flux" as it exits to the ambient environment, similar to that in the flow problem.

2.2 Governing equations

Computation throughout this investigation is based on the three conservation laws: mass, momentum, and energy. A number of assumptions are made, such as steady state, incompressible Newtonian fluid, neglecting gravitation, and 2D axisymmetry. Hence, throughout this study, the buoyancy effect is not taken into account. Air is used as the working fluid with Pr = 0.71. The conservation laws for the current study are as follows:

Continuity equation:

$$\frac{1}{r}\frac{\partial}{\partial r}(rv_r)+\frac{\partial v_z}{\partial z}=0 \tag{1}$$

Momentum equation in radial direction:

$$\rho\left(v_r\frac{\partial v_r}{\partial r}+v_z\frac{\partial v_r}{\partial z}\right)=-\frac{\partial p}{\partial r}+\mu\left[\frac{\partial}{\partial r}\left(\frac{1}{r}\frac{\partial(rv_r)}{\partial r}\right)+\frac{\partial^2 v_r}{\partial z^2}\right] \tag{2}$$

Momentum equation in axial direction:

$$\rho\left(v_r\frac{\partial v_z}{\partial r}+v_z\frac{\partial v_z}{\partial z}\right)=-\frac{\partial p}{\partial z}+\mu\left[\frac{1}{r}\frac{\partial}{\partial r}\left(r\frac{\partial v_z}{\partial r}\right)+\frac{\partial^2 v_z}{\partial z^2}\right] \tag{3}$$

Energy equation:

$$\rho c_p\left(v_r\frac{\partial T}{\partial r}+v_z\frac{\partial T}{\partial z}\right)=k\left[\frac{1}{r}\frac{\partial}{\partial r}\left(r\frac{\partial T}{\partial r}\right)+\frac{\partial^2 T}{\partial z^2}\right] \tag{4}$$

The local heat transfer coefficient is defined as follows:

$$h=\frac{q_s''}{T_s-T_j} \tag{5}$$

The local Nusselt number (Nu) is defined as follows:

$$Nu = \frac{h D_j}{k} \tag{6}$$

Because it is considered a 2D problem, the average Nu is calculated from a length integral.

2.3 Finite element method for the flow field

Once the computational domain was set, unstructured triangle meshes were generated using the Delaunay algorithm, which maximizes the minimum angle of all the angles of the triangles. The circumcircles of a triangle formed by three points from the original point set is empty if it does not contain vertices other than the three that form it. For the incompressible Navier-Stokes, Lagrange elements of order 2 or quadratic elements model the velocity components, and linear elements model the pressure. A second-order Lagrange triangle consists of six node points at the vertices and side midpoints (Fig. 3). For each of these node points P_i, there is a degree of freedom $N_i = n(P_i)$ and basis function ϕ_i. Restriction of the basis function ϕ_i to an element is a polynomial with a degree of 2 in the local coordinates, such that $\phi_i = 1$ at node i and $\phi_i = 0$ at all other nodes. Thus, the basis functions are continuous, as shown in the system of equations below:

$$\phi(x,y) = \sum N_i(x,y)\,\phi_i \tag{7}$$

where ϕ represents basis functions, such as u, v.

The interpolation function N is dependent on a function of area coordinates L_1, L_2, and L_3, as follows:

$$N_1 = L_1^2 - L_1(L_2 + L_3) \quad N_4 = 4L_2L_3$$
$$N_2 = L_2^2 - L_2(L_3 + L_1) \quad N_5 = 4L_3L_1$$
$$N_3 = L_3^2 - L_3(L_1 + L_2) \quad N_6 = 4L_1L_2$$

where $L_i = \frac{1}{2A}(a_i + b_i x + c_i y)$

$$a_1 = x_2y_3 - x_3y_2 \quad b_1 = y_2 - y_3 \quad c_1 = x_3 - x_2$$
$$a_2 = x_3y_1 - x_1y_3 \quad b_2 = y_3 - y_1 \quad c_2 = x_1 - x_3$$
$$a_3 = x_1y_2 - x_2y_1 \quad b_3 = y_1 - y_2 \quad c_3 = x_2 - x_1$$

The variable A represents an area of each element and is calculated from the following equation:

$$A = \frac{1}{2}\left[x_2(y_3 - y_1) + x_1(y_2 - y_3) + x_3(y_1 - y_2)\right]$$

Note that COMSOL developed the code in Cartesian coordinates despite the fact that the computational domain is constructed in cylindrical coordinates.

For pressure distribution on each Lagrange element, the polynomial is of the order of 1, indicating that three nodes are contained on the triangular vertices (labeled 1, 2, and 3; Fig. 3). The basis function is as follows:

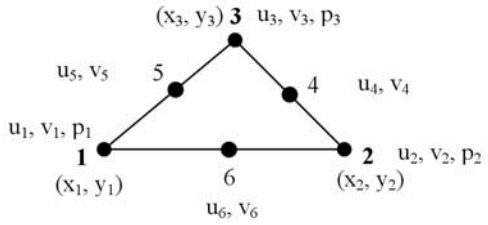

Fig. 3. Labels of nodes and dependent variables for a Lagrange element.

$$p = H_j p_j \text{ ; j = 1,2,3} \tag{8}$$

where H_j is an interpolation function or function of the area coordinates. such that the following hold true:

$$H_1 = L_1 \qquad H_2 = L_2 \qquad H_3 = L_3$$

The Galerkin method was then used, which means that the interpolation function is a weighted function. Applying this function to continuity and x-momentum and y-momentum conservation equations and integrating them gave the following:

$$\int_A H_i\left(\frac{\partial u}{\partial x} + \frac{\partial v}{\partial y}\right)dA = 0 \tag{9a}$$

$$\int_A N_i\left[\rho\left(u\frac{\partial u}{\partial x} + v\frac{\partial u}{\partial y}\right) - \left(2\mu\frac{\partial^2 u}{\partial x^2} - \frac{\partial P}{\partial x} + \mu\frac{\partial^2 u}{\partial y^2} + \frac{\partial^2 v}{\partial x \partial y}\right)\right]dA = 0 \tag{9b}$$

$$\int_A N_i\left[\rho\left(u\frac{\partial v}{\partial x} + v\frac{\partial v}{\partial y}\right) - \left(2\mu\frac{\partial^2 u}{\partial y^2} - \frac{\partial P}{\partial y} + \mu\frac{\partial^2 u}{\partial x \partial y} + \frac{\partial^2 v}{\partial x^2}\right)\right]dA = 0 \tag{9c}$$

Finally, after applying boundary conditions using the UMFPACK algorithm, which is a highly efficient direct solver for asymmetric systems using the asymmetric-pattern multifrontal method and direct LU factorization of the sparse matrix, as a solver with a tolerance of 10^{-6}, matrices of the solution (u, v, p) are obtained.

2.4 Finite element method for the heat transfer

The procedure is similar to that in the previous section, except for the fact that the software uses linear elements (three-node element) to model the heat transfer problem. Applying the Galerkin method to the heat transfer equation yields the following:

$$-\int_A W_i k\left(\frac{\partial^2 T}{\partial x^2} + \frac{\partial^2 T}{\partial y^2}\right)dA + \int_A W_i \rho c\left(u\frac{\partial T}{\partial x} + v\frac{\partial T}{\partial y}\right)dA = 0 \tag{10}$$

where W_i represents the interpolation function. Then, applying the thermal boundary conditions and using the UMFPACK solver, the matrix of temperatures is obtained.

2.5 Meshing

Unstructured meshes or triangular meshes are chosen for the entire study. Meshes near the nozzle exit and the dimple and its edge are denser than anywhere else in the domain. The maximum element size is 1/15 of the maximum distance in the geometry. The element growth rate is 1.3, and the tested mesh densities are 17.32, 21.32, and 23.14 meshes/mm^2. These results are validated in the following section.

3. Validation of flat plate impingement

Validation of the computational results on the flat plate impingement is performed against the experimental results and the computational results from the finite volume method, prior to analyzing the dimple impingement. Appropriate computational domains are selected by taking into account the effects of mesh density and nozzle confinement.

3.1 Validation against experimental results

In this study, the jet exit diameter D_j measures 5 mm, the length (ℓ) of the nozzle is 10 mm, and its thickness is 1 mm. No-slip boundary conditions are given to all walls for the flow problem. Outflow means that the post-impinging jet is leaving the domain to the atmosphere (1 atm). The velocity profile at the nozzle exit is parabolic, and Re is defined as follows:

$$\mathrm{Re} = \frac{\rho D_j U_j}{\mu} \tag{11}$$

where U_j is the average jet exit velocity. For the thermal boundary conditions, the upper plate and the nozzle surface are assigned thermal insulation, and the temperature of the jet issuing from the nozzle is 293 K. The impingement plate has a uniform heat flux of 500 W/m^2. The post-impinging jet then leaves the domain to the atmospheric air. Thermal properties of air are found at 293 K.

According to the finite element analyses of Fagan [10] and Decha-ampai [11], higher mesh density leads to higher accuracy and consumes more computer memory. However, the main concern in the current examination is the limitation in the capacity of the personal computer with the specification of Pentium (R) CPU 3.00 GHz and 2 GB of RAM. COMSOL produces evenly distributed meshes in a particular domain, but different mesh densities can be set. Hence, the optimum mesh density must be determined by testing three values of mesh densities: 17.32, 21.32, and 23.14 meshes/mm^2, which are respectively called models A, B, and C for reference purpose. Fig. 4(a) compares the local Nu obtained from each model. The average Nussult numbers of models A and B are compared to that of model C. Differences between the average Nu of models A and B from those of model C are 0.4937% and 0.2523%, respectively. The local Nus of model B are chosen to be compared with those obtained from experiments of Angioletti [2], as presented in Fig. 4(b), at Re = 1,000 and H/D_j = 4.5. Results are in good agreement, with the difference in the average Nu at 1.0443%.

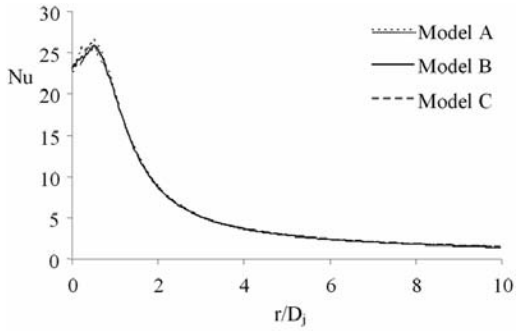

(a) Comparison of local Nus obtained from each model with different mesh densities

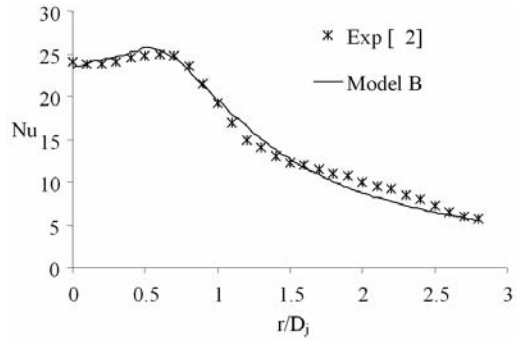

(b) Comparison of local Nus of model B

Fig. 4. Comparison of local Nus with the experimental results of Angioletti et al. [2] at Re = 1,000 and H/D_j = 4.5 after mesh density dependency.

3.2 Validation against results from finite volume method

Because the finite volume method has been used widely, the solution obtained from this study is also compared with those from this method. The work of Chattopadhyay [3] used a SIMPLE algorithm on a 2D axi-symmetric jet impingement. The Re was defined as

$$\mathrm{Re} = \frac{\rho U_j D_j}{\mu} \tag{12}$$

where U_j is the average exit velocity of the jet. Similar to the previous validation, the appropriate model is found when the mesh density and time consumed are considered. In addition, an additional domain is applied in order for the calculation to converge.

The computational domain performed by Chattopadhyay [3] is given as follows: the nozzle length = $0.5D_j$, the distance is measured perpendicularly from the nozzle exit to the impingement plate = $2D_j$, and the impingement plate length = $10D_j$. Furthermore, the nozzle wall is assigned to be a very thin line. The thermal properties of air were set at 303 K.

Set-up of the calculation domain in accordance with Chattopadhyay [3] leads the software to divergence. This is

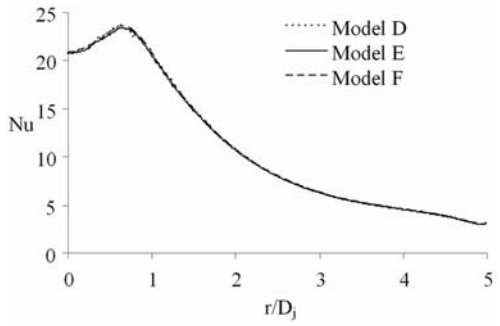

(a) Mesh density dependency check

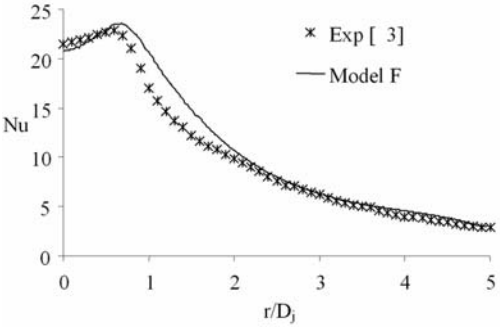

(b) Comparison with experimental results

Fig. 5. Mesh density dependency check on heat transfer and comparison with experimental results of Chattopadhyay [3] at Re = 1,000 and $H/D_j = 2$.

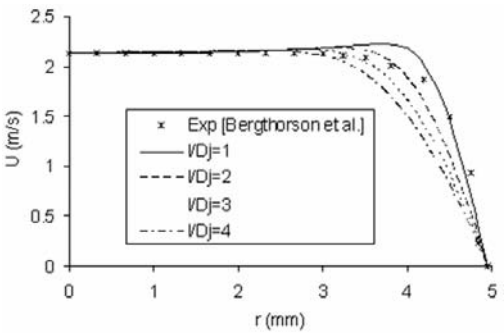

Fig. 6. Comparison of jet exit velocities at the centerline of various values of l/D_j with experimental results of Bergthorson et al. [11] at Re = 1,400.

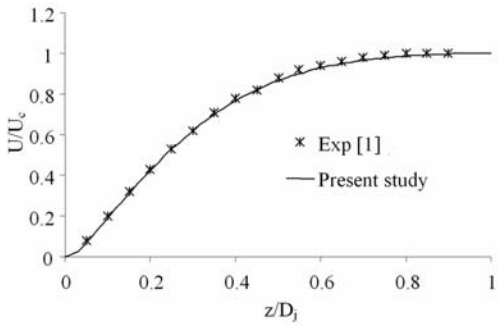

Fig. 7. Comparison of the dimensionless centerline velocities with the results of Bergthorson et al. [1] at Re = 400.

thought to be due to the fact that the length of the impingement surface is too short compared to the jet diameter, causing an end effect. Therefore, an additional domain with the length of $5D_j$ is attached to the first one, which presents new flow and boundary conditions. This does not extend the impingement surface but expands the computational domain. Boundary conditions for the additional domain are set to be exposed to the ambient environment.

The next step is to check mesh density dependency on local Nu by examining three models. The first one, model D, has a mesh density of 35.12 meshes/mm^2 for both domains. The mesh density for model E equals 48.12 meshes/mm^2 for both domains. However, because the first domain is thought to be more significant, the first domain in model F has the same mesh density as that of model E, and the second one is assigned course meshes with a low density of 5.90 meshes/mm^2. The heat transfer results obtained from all three models are plotted in Fig. 5(a), and they show good agreement. Among the three models, model E gives the highest accuracy ([10], [11]) but consumes the highest time and memory. Comparison of the average Nus of models D and F with model E gives 0.3342% and 0.1861%, respectively. Consequently, model F is chosen to validate the results of Chattophadhay [3], as shown in Fig. 5(b), at Re = 1,000 and $H/D_j = 2$. The results agree well near the stagnation zone ($0 < r/D_j < 0.8$) and the wall jet zone starting from $r/D_j > 3$. The difference in the region of $0.8 < r/D_j < 3$ can be due to the fact that the values of the nozzle length and diameter are different. For Re = 500, the difference in the average Nu is 3.6394%, whereas that for Re = 1,000 is 6.8539 %.

3.3 Validation of centerline velocity

Validation begins with comparing computational outcomes with those obtained from Bergthorson et al. [1], who employed an unconfined jet impingement. The results were reported in terms of dimensionless centerline velocity at Re = 400, 700, and 1,400 at $H/D_j = 1$, and Re is defined as follows:

$$\mathrm{Re} = \frac{\rho U_c D_j}{\mu} \tag{13}$$

where U_c represents the jet exit velocity measured at the centerline. The nozzle diameter is given at 9.9 mm, and the diameter of the circular impingement plate is 72.6 mm. The thermal properties of the air jet are observed at 293 K. Length and wall thickness of the nozzle are not given. For the case of unconfined impinging jet, the upper wall is designated as outflow. In addition, it must be sufficiently higher than the nozzle exit to ensure an unconfined problem. Note that due to the lack of information, the nozzle is designed to be cylindrical.

The nozzle lengths of 1, 2, 3, and 4 jet diameters are tested at Re = 1,400 in order to find the appropriate value (Fig. 6). All values give agreeable results along the radial direction with the experimental ones until $r \approx 2.7$. After this,

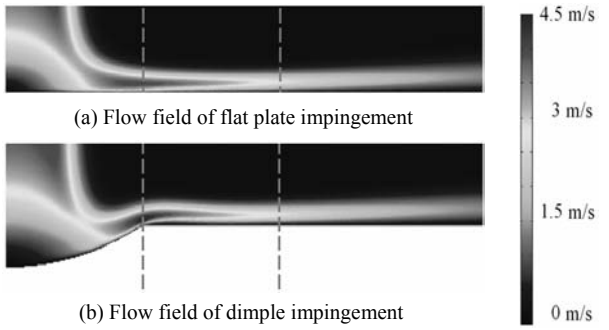

(a) Flow field of flat plate impingement

(b) Flow field of dimple impingement

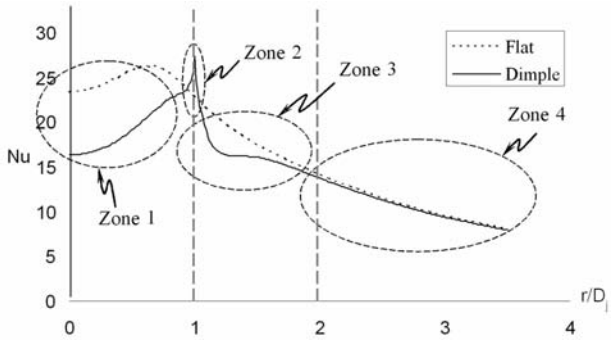

(c) Comparison of local heat transfer and dimple impingement to that of flat plate impingement (circles represent zones of interest)

Fig. 8. Comparison between flat plate and dimple impingement at Re = 1,200 and $H/D_j = 2$ and the dimpled surface of $d/D_d = 0.15$ and $D_j/D_d = 0.5$.

the position of the nozzle of $l/D_j = 2$ provides the best result with a 6.9994% difference from literature. This is subsequently selected for further investigation. In addition, validation for Re = 400 (Fig. 7) and 700 is also tested, and both cases are consistent with the experimental results.

4. Results and discussions

Since experimental data for a laminar jet impinging on a dimpled surface are not available, computational results for dimple impingement in the current study are presented without validation. However, mesh density in the vicinity of a dimple is higher than that in other places of the domain to maintain good accuracy. Apart from comparing the heat transfer results of dimple impingement to those of the flat plate, various parameters were considered, such as the Re, H/D_j, d/D_d, and ratio of jet diameter and dimple projected diameter (D_j/D_d).

4.1 Comparison with flat plate impingement

Fig. 8 shows a comparison of local heat transfer and flow field of the jet impinging on the dimpled surface for $d/D_d = 0.15$ and $D_j/D_d = 0.5$ with that on the flat plate at Re = 1,200, $H/D_j = 2$. Zone 1, which was circled in Fig. 8(c), shows the results of the stagnation region, where flat plate impingement gives a higher heat transfer than that of the dimple impingement. Due to the dimple curvature, the post-impinging fluid

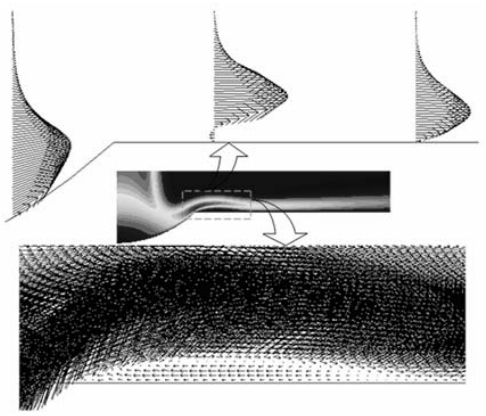

Fig. 9. Velocity profiles in the vicinity of the flat portion adjacent to the dimple.

attempts to traverse downstream, leading to excessive momentum loss near the dimple wall. Thus, its flow velocity gradients become negative. The surface discontinuity presented by the dimple edge in zone 2 causes the high velocity region in Fig. 8(b) and the local heat transfer jump in Fig. 9(c). In zone 3, the local Nu abruptly drops compared to that of the flat plate because the flow separation or back flow is found (Fig. 9). Finally, in zone 4, heat transfer results and flow fields for both cases are similar. The average Nu for the flat plate is 16.6334662, whereas that for the dimpled plate is 14.518827.

4.2 Mesh density independence check

Due to the lack of experimental data for jet impinging on a dimple, mesh density independence check was introduced. Fig. 10(a) shows a comparison of the centerline velocities for the case of Re = 1,200, $H/D_j = 2$, $d/D_d = 0.1$, and $D_j/D_d = 0.5$ at various mesh densities of 17.09 meshes/m, 34.67 meshes/m, and 107.12 meshes/mm^2, which are labeled S, T, and U, respectively. The results are in good agreement. Compared to the data of model U, model S gives a 1.7601% difference, and model T yields a 0.6428% difference. Furthermore, Fig. 10(b) shows a comparison of the Nus for the same case. The vicinity of the dimple is quite crucial because model S does not collapse, compared to the others. Data from models T and U agree well and have a 1.0781% difference, whereas model S is 4.1954% different from that of model U. Therefore, for the entire study on dimple jet impingement, model U with a mesh density of 107.12 meshes/mm^2 was employed.

4.3 Effect of Reynolds number

Although the influence of Reynolds number (Re) on the heat transfer of jet impingement is commonly known, it is still worth investigating. According to Polat [12], a fully developed jet takes place when Re is greater than 3,000. In this study, the Re's tested are in the range of 400-1,200. Fig. 11 shows the local heat transfer of various Re values for $H/D_j = 2$, $d/D_d = 0.2$, and $D_j/D_d = 0.5$. A Re of 1,200 leads to the highest

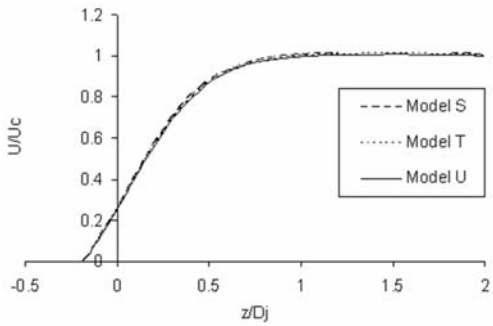

(a) Comparison of centerline velocities from models with different mesh densities

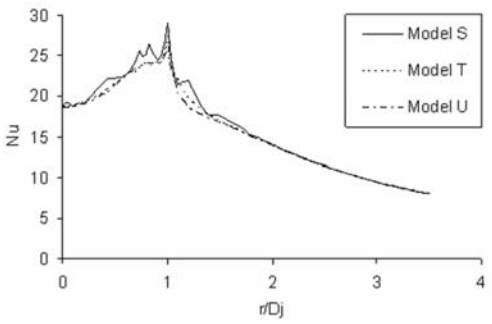

(b) Comparison of local Nus

Fig. 10. Mesh density independence check for dimple impingement: Re = 1,000; H/D_j = 2; d/D_d = 0.15; D_j/D_d = 0.5.

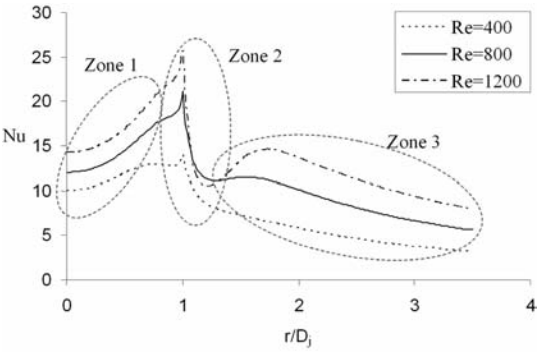

(a) Local Nu distribution divided into three zones

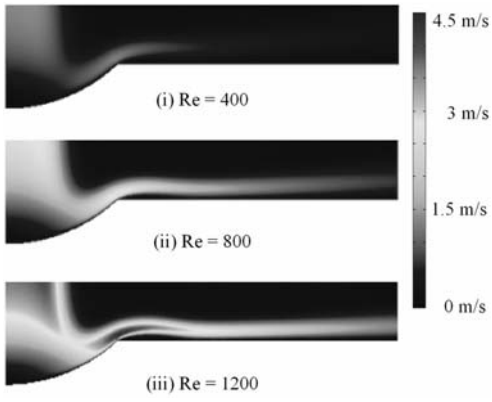

(b) Flow fields of dimple impingement

Fig. 11. Dimple impingement at various Re for H/D_j = 2, d/D_d = 0.2, and D_j/D_d = 0.5.

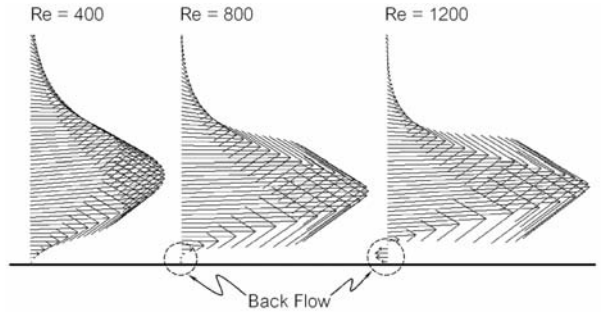

Fig. 12. Velocity profiles for various Re.

heat transfer everywhere, except for the vicinity of the dimple edge where the wall jet begins to form. This is because the oncoming jet with Re = 1,200 carries the highest momentum and thus exchanges that with the target area in the stagnation zone (zone 1). Afterwards, the post-impinging jet accelerates to escape from the indentation toward zone 2. Crossover points are detected in this zone between the Nu plots of Re = 800 and 1,200. This is because the boundary layer flow for Re = 1,200 undergoes adverse pressure gradient earlier and consumes more momentum than that for Re = 800. Therefore, the flow for Re = 1,200 decelerates faster. In addition, close-up velocity profiles on the flat portion next to the dimple in Fig. 12 shows backflow in both cases. Finally, when the wall jet reaches the flat surface (zone 3), Re = 1,200 gives the highest heat transfer, followed by Re = 800 and Re = 400. The flow is similar to a laminar layer flow past a flat plate.

4.4 Effect of jet-to-plate spacing

Fig. 13 presents the local heat transfer distribution for jet impingement on a dimpled plate of d/D_d = 0.1 and D_j/D_d = 0.5 at Re = 1,200 for various values of jet-to-plate spacing (H/D_j). The curves almost collapse, except at the stagnation region, where H/D_j = 8 gives a slightly higher heat transfer result than those of H/D_j = 2 and 4. The flow fields in Fig. 18 suggests that the width of the stagnation region represented by the blue color, or the low velocity zone for the case of H/D_j = 8, is smaller than the other two cases. Moreover, the jet width upon the target surface for H/D_j = 8 is relatively larger because of the expansion of the jet. In addition, because the jet is laminar, it transfers a small amount of momentum to the stagnant surrounding air on its way toward the target surface. In the wall jet zone, the local Nu distribution shows a collapse of all three cases.

4.5 Effect of dimple depth

Dimple depth (d/D_d) remarkably influences heat transfer of the impinging jet on a dimpled plate. This is shown in the plots of local Nus for all tested values of d/D_d for Re = 1,200, H/D_j = 4 and D_j/D_d = 0.5 (Fig. 14). A significant difference can be observed in the stagnation zone (Zone 1). However, the heat transfer values are similar at the dimple edge. They then decrease in the adjacent flat portions, where backflow is

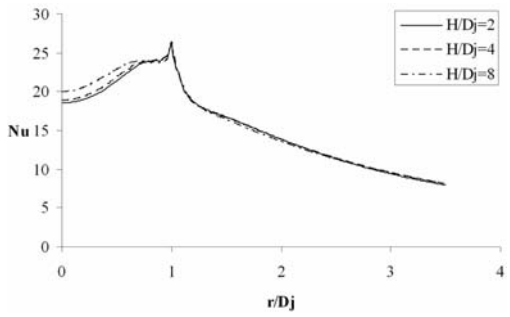

(a) Local Nus

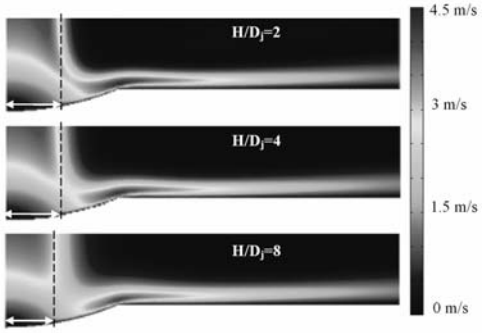

(b) Flow fields

Fig. 13. Dimple impingement at different H/D_j for Re = 1,200, d/D_d = 0.1, and D_j/D_d = 0.5.

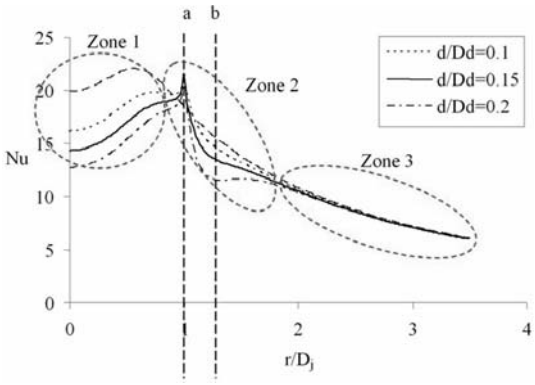

(a) Local Nu distribution zoning

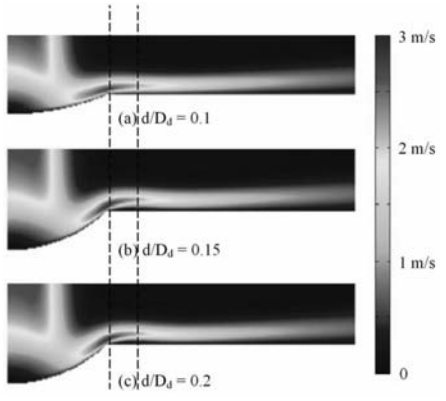

(b) Flow fields

Fig. 14. Comparison of jet impingement on different d/D_d and flat plate for Re = 1,200, H/D_j = 4, and D_j/D_d = 0.5.

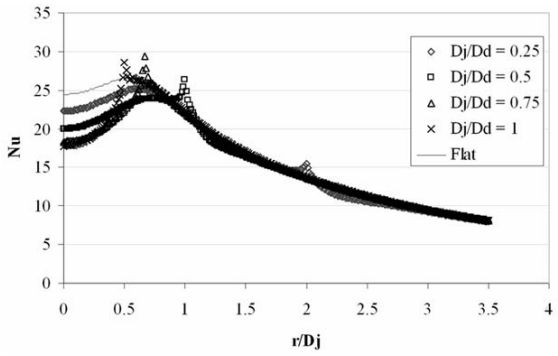

(a) Local Nus for cases of flat plate and dimple impingement

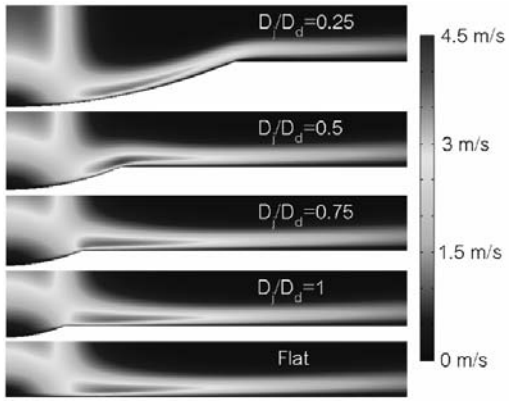

(b) Flow fields

Fig. 15. Local Nu distribution and flow fields for different ratios of jet diameter to dimple projected diameter (D_j/D_d) for Re = 1,200, H/D_j = 8, and d/D_d = 0.1.

acquired. Afterwards, the local heat transfer curves collapse. The deepest dimple of d/D_d = 0.2 gives the lowest heat transfer because of the highest degree of curvature, from which fluid escapes with more difficulty, causing the fluid to lose more momentum. Hence, a higher degree of flow separation occurs at the deeper dimple. The average Nus for d/D_d = 0 (flat plate), 0.1, 0.15, and 0.2 are 16.633466, 15.568294, 14.785281, and 13.427107, respectively.

4.6 Effect of ratio of jet diameter to dimple projected diameter

The tested ratios of jet diameter to dimple projected diameter are 0.25, 0.5, 0.75, and 1.0, measured by varying D_d and fixing D_j at 5 mm. The heat transfer results in Fig. 15(a) show a strong influence of D_j/D_d, especially in the stagnation zone. The figure also presents a comparison with the flat plate impingement. For all four values of D_j/D_d, the curves can be grouped into two shapes. The first group resembles that of the flat plate, except where the dimple edge appears: D_j/D_d = 0.25 and 0.5. Also, the oncoming jet impinges entirely inside the dimple. The second group is for those where the stagnation zone covers the entire dimple: D_j/D_d = 0.75 and 1.

Considering group 1 (impingement inside the dimple), even though the local heat transfer curve shapes of $D_j/D_d = 0.25$ and 0.5 are similar to that of the flat plate, the levels of heat transfer are less. A remarkable difference in the result is found at the dimple edge position, where the local heat transfer jumps. Because the dimple edge for $D_j/D_d = 0.5$ appears earlier than that for $D_j/D_d = 0.25$, the jump occurs earlier in the high-velocity zone, as shown by its flow field in Fig. 15(b), causing high loss in momentum. In contrast, the dimple edge of $D_j/D_d = 0.25$ occurs in the low-momentum zone as displayed in the yellowish region in the flow field. Thus, its jet loses less momentum than $D_j/D_d = 0.5$.

Group 2 represents the case of the impingement zone covering the entire dimple, and this occurs to the impingement on $D_j/D_d = 0.75$ and 1. As aforementioned, presence of the dimple edge causes heat transfer reduction compared to transfer on the flat plate because the fluid attempts to escape from the curvature. Significant heat transfer reduction occurs in the stagnation zone. After jumping at the dimple edge, the local heat transfer curve collapses to that of the flat plate heat transfer.

5. Conclusions

This study uses the commercial software package called COMSOL that uese a finite element method to process the flow and heat transfer problems of an axi-symmetric laminar jet impinging on a flat and a dimpled surface. The work is divided into two main parts: (1) validation of the software against the experimental results obtained from literature and (2) investigation of parametric effects on dimple impingement.

For the validation, only results from flat plate impingement were compared to the experimental and computational results obtained from literature. The effect of mesh density dependency was closely examined. Mesh density does not affect heat transfer and flow problems. However, the mesh densities that help save computational memory and time were selected. Experimental and computational results obtained from literature were compared with those from the current investigation, and a good agreement was found.

Various parametric effects of dimple impingement were considered, such as Re, H/D_j, d/D_d, and the ratio of dimple projected diameter and jet diameter (D_j/D_d):

The Re significantly affects heat transfer of the dimple impingement. An oncoming jet with higher Re carries a higher amount of momentum, so the stagnation heat transfer is higher.

H/D_j does not significantly affect heat transfer because the oncoming viscous laminar jet exchanges a small amount of momentum with the ambient air before impinging on the target plate.

A deeper dimple presents a decrease in heat transfer because the dimple possesses a higher degree of curvature, as well as a larger wetted area. The larger wetted area, thus, leads to less momentum flux.

When considering the influence of D_j/D_d, heat transfer results can be divided into two groups: (1) jet impinging within the dimple and (2) impinging jet covering the dimple. The first case has a similar local Nu distribution trend as that of the flat plate, except where the dimple is present, at which point mild heat transfer reduction is found. The second group gives a higher degree of heat transfer reduction, which occurs at the indentation.

Finally, heat transfer results of dimple impingement were compared to those of flat plate impingement. Heat transfer reduction occurs in the vicinity of the indentation and the dimple edge. The flow fields show that the dimple edge lifts the post-impinging jet, and backflow is found in some cases of dimple impingement. Thus, the presence of a dimple causes overall heat transfer reduction to a laminar impinging jet.

Acknowledgements

This research is financially supported by the Thailand Research Fund (TRF), whose guidance and assistance are gratefully acknowledged. The authors thank Dr. Markus Huebscher for providing relevant documents. In addition, the third author would like to thank King Mongkut's University of Technology Thonburi and the Office of the Higher Education Commission for their support.

Nomenclature

d : Dimple depth, m
g : Gravitation acceleration, m/s^2
h : Heat transfer coefficient
k : Jet thermal conductivity
l : Nozzle length, m
p : Pressure, Pa
q" : Heat flux, W/m^2
r : Radial direction
v : Velocity, m/s
z : Axial direction
A : Area of an element
D : Diameter, m
H : Distance between nozzle exit and target plate (flat portion level for dimpled plate)/Interpolation function for pressure
L : Area coordinates of an element
N : Interpolation function for velocities
Nu : Nusselt number, $\frac{hD_j}{k}$
Re : Reynolds number, $\frac{\rho UD_j}{\mu}$
S : Nozzle thickness, m
W : Interpolation function for temperature

Subscripts

c : Centerline
d : Dimple plate

i : Index for node in an element
j : Jet
s : Of surface

Greek symbols

ϕ : Basis function
μ : Jet viscosity
ρ : Jet density

References

[1] J. M. Bergthorson, K. Sone, T. W. Mattner, P. E. Dimotakis, D. G. Goodwin and D. I. Meiron, Impinging laminar jets at moderate Reynolds numbers and separation distances. *Phy. Rev. E*, 72 (6) (2005) 066307-1-12.

[2] M. E. Angioletti, E. Nino and G. Ruocco, CFD turbulent modelling of jet impingement and its validation by particle image velocimetry and mass transfer measurements, *Int. J. Ther.* Sc. 44 (2005) 349-356.

[3] H. Chattopadhyay, Numerical investigations of heat transfer from impinging annular jet, *Int. J. Heat Mass* 47 (2004) 3197-3201.

[4] L. B. Y. Aldabbagh and I. Sezai, Three-dimensional numerical simulation of an array of impinging laminar square jets with spent fluid removal, *Int. J. Ther. Sc.* 43 (2004) 241-247.

[5] Gm., S. Azad, Y. Huang and J. Han, Impingement heat transfer on dimpled surfaces using a transient liquid crystal technique, *J. Thermophy Heat Tran.* 14 (2000) 186-193.

[6] S. V. Ekkad and D. Controvitz, Jet impingement heat transfer on dimpled target surfaces, *Int. J. Heat Fluid Flow,* 23 (2002) 22-28.

[7] K. Kanokjaruvijit and R. F. Martinez-Botas, Jet impingement on a dimpled surface with different crossflow schemes, *Int. J. Heat Mass Tran.* 48 (2004) 161-170.

[8] K. Kanokjaruvijit and R. F. Martinez-Botas, Parametric effects of heat transfer of impingement on dimpled surface, *J. Turbomach.* 127 (2005) 287-296.

[9] K. Kanokjaruvijit and R. F. Martinez-Botas, Heat Transfer and pressure investigation of dimple impingement, *J. Turbomach.* 130 (2008) 011003-1-9.

[10] M. J. Fagan, Finite element analysis: theory and practice, Prentice Hall, New Jersey, (1992).

[11] P. Decha-ampai, Finite element method for fluid dynamics (in Thai), Chulalongkorn Press, Bangkok, Thailand, (2002).

[12] S. Polat, B. Huang, A. S. Mujumdar and W. J. M. Douglas, Numerical flow and heat transfer under impinging jets: a review, Annual review of Numerical Fluid Mechanics and Heat Transfer, 2 (1989) 157-197.

Koonlaya Kanokjaruvijit received her PhD in Mechanical Engineering from Imperial College London, UK in 2004. She is now an assistant professor at Naresuan University, Phitsanulok Thailand. Her research interests include design of cooling schemes in gas turbine engine and hemodynamics

Chakkraphan Thawonngamyingsakul is a lecturer in the Department of Mechanical Engineering, Rajamangala University of Technology Lanna Tak, Thailand. He received his MEng in Mechanical Engineering from Naresuan University, Thailand in 2007. His research is in thermal system design and heat transfer enhancement. He is currently pursuing a PhD in Energy Engineering at Chiengmai University, Thailand.

Somchai Wongwises is currently a Professor of Mechanical Engineering at King Mongkut's University of Technology Thonburi, Bangmod, Thailand. He received his Doktor Ingenieur (Dr.-Ing.) in Mechanical Engineering from the University of Hannover, Germany, in 1994. His research interests include Gas-Liquid Two-Phase Flow, Heat Transfer Enhancement, and Thermal System Design. Professor Wongwises is the head of the Fluid Mechanics, Thermal Engineering and Multiphase Flow Research Laboratory (FUTURE).